Contrast Reversal in Atomic-Resolution Chemical Mapping

P. Wang,[1] A. J. D'Alfonso,[2] S. D. Findlay,[3] L. J. Allen,[2] and A. L. Bleloch[1]
[1]UK SuperSTEM Laboratory, Daresbury Laboratory, Cheshire WA4 4AD, United Kingdom
[2]School of Physics, University of Melbourne, Parkville, Victoria 3010, Australia
[3]Institute of Engineering Innovation, School of Engineering, University of Tokyo, Tokyo, 113-8656, Japan
(Received 29 August 2008; published 2 December 2008)

We report an unexpected result obtained using chemical mapping on the new, aberration corrected Nion UltraSTEM at Daresbury. Using different energy windows above the $L_{2,3}$ edge in ⟨011⟩ silicon to map the position of the atomic columns we find a contrast reversal which produces an apparent and misleading translation of the silicon columns. Using simulations of the imaging process, we explain the intricate physical mechanisms leading to this effect.

DOI: 10.1103/PhysRevLett.101.236102 PACS numbers: 68.37.Lp, 61.85.+p, 79.20.Uv

A complete characterization of a natural or synthetic material requires identifying the atoms, their positions, and bonding interactions. Until recently this has been achieved by diffraction techniques which average over many identical atomic arrangements [1,2]. Our ability to engineer materials at the atomic scale creates an increasing need to do such mapping locally in real space. Just such chemical mapping has been demonstrated in the past year using high resolution scanning transmission electron microscopy (STEM) [3–5]. An Ångström-sized probe is raster scanned across the sample and electron energy-loss spectroscopy (EELS) data are recorded to provide chemical identification and explore local bonding and other electronic properties. Simultaneously recording electrons which have been scattered through large angles after exciting a crystal phonon, *Z*-contrast or high angle annular dark field (HAADF) imaging, provides a reference image for the position of the columns [6–10]. The extension of chemical mapping to three dimensions via tomographic techniques is currently being pursued [11,12]. We report an unexpected result obtained in chemical mapping on the new, fifth order aberration corrected, 100 keV Nion UltraSTEM at Daresbury that has important consequences for the interpretation of the location of atom columns, supporting suggestions that high resolution STEM images may not always admit direct visual interpretation [13,14]. Using different energy windows above the $L_{2,3}$ edge in ⟨011⟩ silicon to map the position of the atomic columns we find a contrast reversal, leading to an apparent translation of the columns.

This study used a ⟨011⟩ silicon cross-sectional specimen that was conventionally prepared by mechanical polishing followed by brief argon ion-milling at TU Chemnitz. The sample was estimated to be 910 Å thick. The convergence semiangle of the 100 keV Nion UltraSTEM was 24 mrad. The simultaneous HAADF image, Fig. 1(a), was obtained using a 105–300 mrad annular collection range. The Nion UltraSTEM was equipped with a Gatan Enfina electron energy-loss spectrometer that has a collection semiangle of 67 mrad in the spectrometer's energy dispersive direction and 22 mrad in the non–energy dispersive direction. A dispersion of 0.5 eV/channel was selected and the dwell time was set to 5 msec/spectrum. The charge on the CCD detector was binned from 100 into 20 channels in the non–energy dispersive direction. The entire spectrum image of 20×20 pixels was recorded in 17 seconds with dark current and gain normalization. A 20×16 pixel subset is show in Figs. 1(b) and 1(c) for energy-loss windows of 143–163 eV and 280–300 eV subsequent to background subtraction. The power-law background fitting was sampled within a 20 eV window on the low-energy side of the Si $L_{2,3}$ edge. A typical example of the energy-loss spectrum, depicting the background subtraction and the selected energy windows, is shown in Fig. 1(d).

Theoretical calculations supporting the experimental results were carried out using the Bloch wave method [15]. The projected atomic transition potentials were calculated using relativistic Hartree-Fock bound and Hartree-Fock-Slater continuum states assuming the central field approximation (i.e., radial symmetry). The effect of the crystal potential on the ejected atomic electron can be neglected—we integrate over a 20 eV energy window. Calculations predict that the contribution of electrons that excite L_1-ionizations is over an order of magnitude smaller than those that excite $L_{2,3}$ ionizations, and so the former are neglected. The large extent of the post-specimen detector permitted the approximation that the inelastic wave decoupled to plane waves post interaction [16]. The 24 mrad probe forming aperture was modelled as being aberration free. The simulations accounted for the spatial incoherence of the probe via convolution of the image with a Gaussian of half-width-half-maximum 0.6 Å [17]. This number no longer allows for resolution of the 1.4 Å silicon dumbbell spacing for the ⟨011⟩ projection in the simulated HAADF image, in agreement with the experimental results. An Einstein model for thermal scattering was used to calculate the scattering into the HAADF detector, and also to model the absorptive effect on the elastic probe.

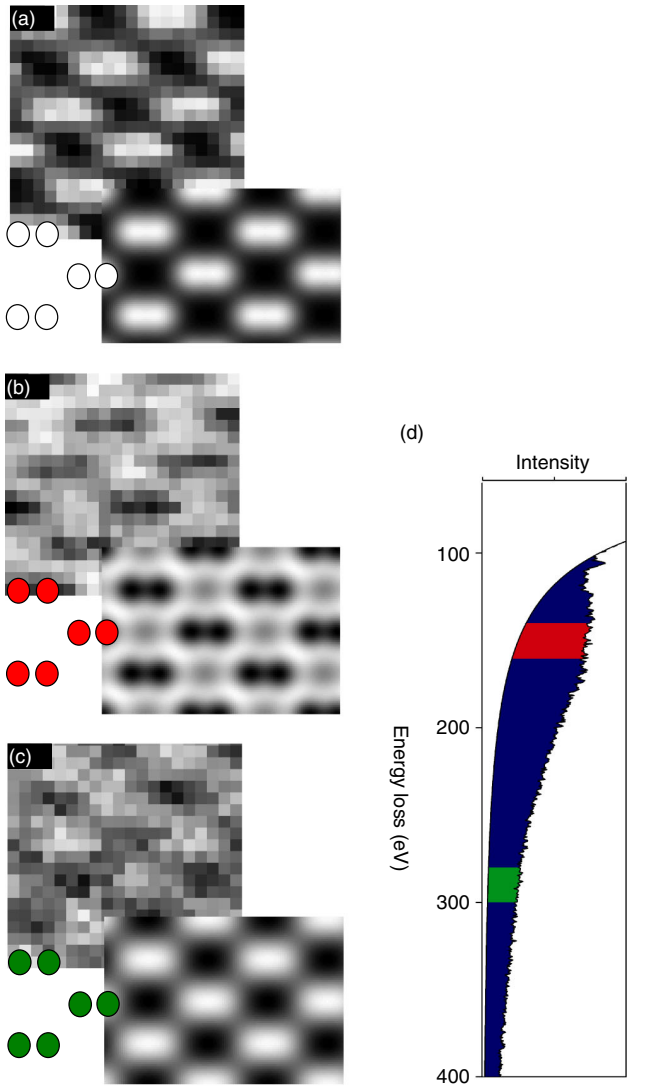

FIG. 1 (color online). Comparison between experimental (underlay) and simulated (overlay) images of ⟨011⟩ Si. (a) HAADF, (b) 143–163 eV energy filtered EELS, and (c) 280–300 eV energy filtered EELS images. (d) A typical acquired Si EELS spectrum showing the background fit curve subtraction. The energy windows are color coded with the indicated atomic structures on the corresponding images. All images were acquired simultaneously.

The projected dumbbell structure formed by adjacent columns of silicon atoms is correctly shown by the experimental (underlay) and simulated (overlay) HAADF images in Fig. 1(a). The $L_{2,3}$-shell EELS images for the energy windows 143–163 eV and 280–300 eV in Figs. 1(b) and 1(c) are obtained simultaneously with the HAADF image, and thus the electron probe experiences identical scattering and absorption conditions. We note that while the columns for the 280–300 eV energy window image are in register with the HAADF image, correctly reflecting the known structure, in the 143–163 eV energy window image the columns have apparently been translated.

Since the evolution of the electron probe through the specimen is identical in both images, the difference must arise from the variation of the ionization interaction with energy loss. The ionization probability is known to become increasingly localized with increasing energy loss [18]. Using experimental data for this same edge, though in a thinner Si_3N_4 specimen, Kimoto *et al.* [19] recently demonstrated this effect in 2D EELS images. We can assess the variation in localization directly and quantitatively by exploring the dependence of the localization of the inelastic transition potential on energy loss [20]. The inelastic wave function is proportional to the product of the transition potential and the elastic wave function, so the modulus squared of the transition potentials measures the strength of the transfer of electron density into the inelastic channels. Figure 2(a) shows the modulus squared of the inelastic transition potentials from an initial state with quantum numbers $l = 1$, $m_l = 0$ to a final state with quantum numbers $l' = 2$, $m'_l = 0$ as a function of energy loss for the Si $L_{2,3}$ edge. While the width of the potential over the 280–300 eV window is comparable to the interdumbbell spacing, over the 143–163 eV window the potential is much more delocalized. The manner in which this variation affects the STEM EELS images depends on how the widths of these potentials compares with the distribution of the probe wave function at the various energies. For our fine probe and relatively thick but weakly scattering specimen, probe spreading is significant. This is illustrated by the radially integrated probe intensity shown in Fig. 2(b), where the intensity distribution for the probe placed on an open channel is seen to spread quite rapidly.

The consequences of this probe diffusion on the images is shown in Figs. 2(c) and 2(d), where we plot the EELS line scan along the axis of the silicon dumbbells as a function of thickness for the two different energy-loss windows. Spatial incoherence has been omitted here to concentrate solely on the channelling and delocalization aspects. The first point to note is that the contrast is quite low for a wide range of thickness values, a consequence of the significant delocalization of the potential. Kimoto *et al.* [19] suggested that such delocalization might prevent atomic-resolution imaging. As seen in Fig. 1 and for certain depths in Figs. 2(c) and 2(d), atomic scale features can sometimes be seen clearly above the "delocalized background." Moreover, we find cases where the correspondence between atomic scale features and the true atomic structure changes depending on the delocalization. The change in the EELS image contrast is a subtle competition between the elastic and inelastic scattering as a function of the probe position. General principles for how the balance between these aspects plays out remain elusive, making simulation an often essential part of atomic-resolution chemical mapping.

The usual approach to EELS imaging uses a large energy window directly above the ionization threshold. The large width maximizes the signal while proximity to the

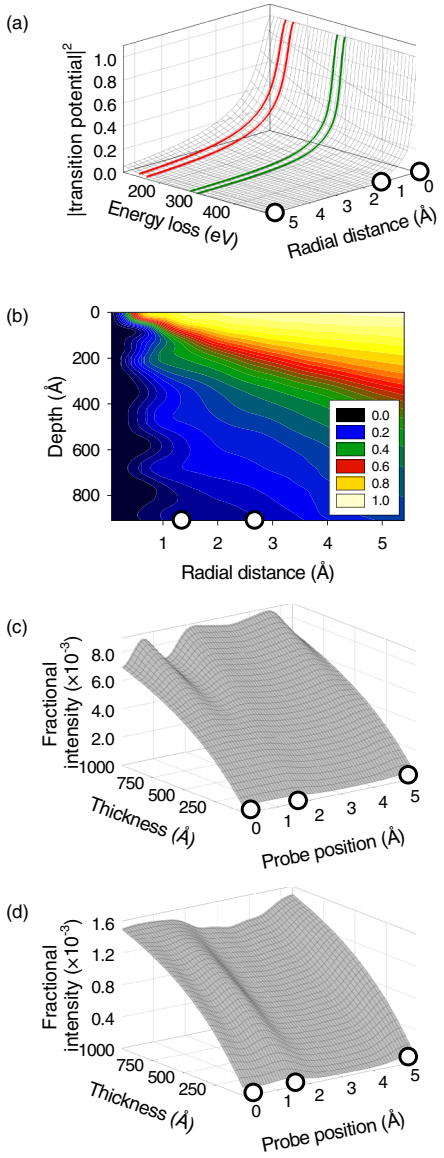

FIG. 2 (color online). (a) Modulus squared of the transition potentials, normalized to unity at the origin for a clear comparison of the change in shape, from initial state $l = 1$, $m_l = 0$ to final state $l' = 2$, $m_l' = 0$ as a function of energy loss for an isolated Si atom. The 143–163 eV and 280–300 eV energy windows are indicated. Circles show the locations of columns along [100]. (b) Proportion of the electron probe intensity as a function of radial distance from the probe origin when the probe is placed at $(x, y) = 4.07, 0.00$ Å (off column). Cumulative contribution to the Si $L_{2,3}$-shell EELS signal for Si $\langle 011 \rangle$ scanning along the [100] direction for energy-loss windows of (c) 143–163 eV and (d) 280–300 eV.

edge makes the background subtraction, based on extrapolation of the preedge, as reliable as possible. Figure 3 shows the integration of the modulus squared of the $l = 1$, $m_l = 0$ to $l' = 2$, $m_l' = 0$ transition potentials as a function of radial distance over energy windows of width 10 eV and 40 eV and starting at three different initial values of energy loss. The integrated potential becomes notably

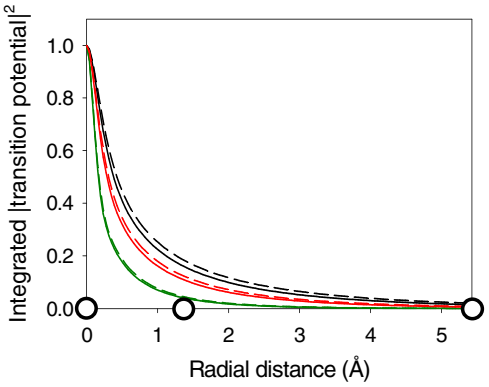

FIG. 3 (color online). Integrated modulus squared of the transition potentials for the $l = 1$, $m_l = 0$ to $l' = 2$, $m_l' = 0$ transition as a function of radial distance for energy windows of width 10 eV (solid lines) and 40 eV (dashed lines), starting at three different initial values of energy. The top two lines are for windows starting at the ionization edge, 100 eV, the next two lines are for windows starting at 143 eV, and the bottom two are for an initial energy value of 280 eV. The results are all normalized to unity at the origin to better observe the variation in shape.

more localized for increasing energy loss. The energy window near threshold encompasses the most delocalized potentials and so gives the least resolvable images. With respect to localization, one should place the energy window as far above threshold as the background subtraction procedure justifiably allows. Kimoto *et al.* reached the same conclusion [19]. The main effect on the localization of the long range behavior of the potential is the energy loss rather than the specific atomic states involved in the transition [21]: the effect is strongly pronounced here because the ionization threshold energy is low. For an element and shell with a much higher ionization threshold, the variation in localization with energy loss will be much weaker. It is clear from Figs. 2(a) and 3 that the size of the energy-loss window only affects the localization if strong variation in the localization of the potential occurs on a smaller energy scale.

Two further points are needed to fully appreciate what is occurring with this data set. First, if the effect of inelastic thermal scattering on the evolution of the elastic wave function is neglected then the simulations do not show a contrast reversal. This suggests that thermal scattering appreciably modifies the evolution of the probe wave function, despite the generally weak scattering power of silicon atoms, and that the absorption effect (i.e., thermal scattering prior to the excitation of ionization events) may in part be contributing to the reduction of the signal on column [3]. That this might lead to a contrast reversal depending on the energy loss has been predicted previously (albeit for different edges) [22], but has not hitherto been seen experimentally. Second, attributing the contrast reversal to probe spreading depends on the excitation of atoms in multiple columns, which has previously been

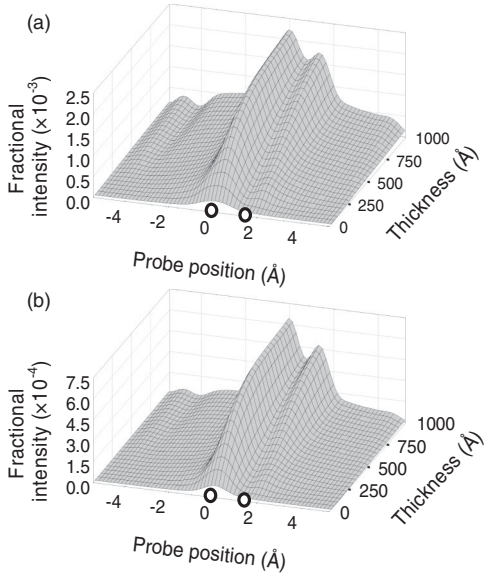

FIG. 4. The cumulative contribution from a single column located at $x = 0.0$ Å using (a) 143–163 eV and (b) 280–300 eV integration windows for a line scan through the Si dumbbells.

dubbed cross-talk (see, for instance, Refs. [13,15]). We can elucidate this by a trial calculation in which only silicon atoms in a single column are allowed to undergo ionization. Such an approach retains the physically correct evolution of the wave function, while analyzing the contribution to the EELS signal from only a subset of atoms. This dissection is physically meaningful because core-loss ionization of different atoms is regarded as being incoherent. The resultant signal as a function of specimen thickness is given in Figs. 4(a) and 4(b). For both energy-loss ranges the ionization signal from that single column is a maximum when the probe is on that column. As the line scans shown in Figs. 2(c) and 2(d) result from the superposition of such single column signals, the addition of the intercolumnar contribution from adjacent columns reduces the overall contrast and is directly responsible for the observed contrast reversal.

In summary, while undertaking atomic-resolution 2D chemical mapping using electrons from different regions of the silicon core-loss spectrum we found a contrast reversal from within the *same* ionization edge. For our fine probe and relatively thick but weakly scattering specimen, simulation shows that this unexpected result arises because probe spreading from an open channel ultimately allows for more interaction with the delocalized transition potentials of more silicon atoms than when it is placed upon a column. Whilst the reversal is observed in an area of the sample that was relatively thick, good HAADF images and EELS spectra were obtained; while the contrast is low, reliable signal variation is seen. For the most delocalized potentials atomic scale features do not always reliably represent the atomic scale structure. Detailed theoretical understanding of measured results can avoid interpretive pitfalls in atomic scale chemical mapping by high spatial resolution electron energy-loss spectroscopy.

P. W. and A. L. B. acknowledge financial support from the EPSRC for the SuperSTEM project. L. J. A. acknowledges support from the Australian Research Council. S. D. F. received support from the Japanese Society for the Promotion of Science.

[1] J. C. H. Spence and J. M. Zuo, *Electron Microdiffraction* (Plenum Press, New York, 1992).
[2] L. Reimer, *Transmission Electron Microscopy* (Springer-Verlag, Berlin, 1984).
[3] M. Bosman, V. J. Keast, J. L. García-Muñoz, A. J. D'Alfonso, S. D. Findlay, and L. J. Allen, Phys. Rev. Lett. **99**, 086102 (2007).
[4] K. Kimoto, T. Asaka, T. Nagai, M. Saito, Y. Matsui, and K. Ishizuka, Nature (London) **450**, 702 (2007).
[5] D. A. Muller, L. Fitting Kourkoutis, M. Murfitt, J. Song, H. Hwang, J. Silcox, N. Dellby, and O. Krivanek, Science **319**, 1073 (2008).
[6] N. D. Browning, M. F. Chisholm, and S. J. Pennycook, Nature (London) **366**, 143 (1993); **444**, 235(E) (2006).
[7] D. A. Muller, Y. Tzou, R. Raj, and J. Silcox, Nature (London) **366**, 725 (1993).
[8] P. E. Batson, Nature (London) **366**, 727 (1993).
[9] E. M. James and N. D. Browning, Ultramicroscopy **78**, 125 (1999).
[10] M. Varela, S. D. Findlay, A. R. Lupini, H. M. Christen, A. Y. Borisevich, N. Dellby, O. L. Krivanek, P. D. Nellist, M. P. Oxley, and L. J. Allen *et al.*, Phys. Rev. Lett. **92**, 095502 (2004).
[11] K. van Benthem, A. R. Lupini, M. Kim, H. Suck Baik, S. J. Doh, J. Lee, M. P. Oxley, S. D. Findlay, L. J. Allen, and J. T. Luck *et al.*, Appl. Phys. Lett. **87**, 034104 (2005).
[12] L. J. Allen, Nature Nanotech. **3**, 255 (2008).
[13] C. Dwyer and J. Etheridge, Ultramicroscopy **96**, 343 (2003).
[14] M. P. Oxley, E. C. Cosgriff, and L. J. Allen, Phys. Rev. Lett. **94**, 203906 (2005).
[15] L. J. Allen, S. D. Findlay, M. P. Oxley, and C. J. Rossouw, Ultramicroscopy **96**, 47 (2003).
[16] C. Dwyer, S. D. Findlay, and L. J. Allen, Phys. Rev. B **77**, 184107 (2008).
[17] P. D. Nellist and J. M. Rodenburg, Ultramicroscopy **54**, 61 (1994).
[18] R. F. Egerton, *Electron Energy-Loss Spectroscopy in the Electron Microscope* (Plenum Press, New York, 1996), 2nd ed.
[19] K. Kimoto, K. Ishizuka, and Y. Matsui, Micron **39**, 257 (2008).
[20] C. Dwyer, Ultramicroscopy **104**, 141 (2005).
[21] D. A. Muller and J. Silcox, Ultramicroscopy **59**, 195 (1995).
[22] S. D. Findlay, M. P. Oxley, S. J. Pennycook, and L. J. Allen, Ultramicroscopy **104**, 126 (2005).